

# Spectroscopy of Red Giants in the globular cluster Terzan 8: kinematics and evidence for the surrounding Sagittarius stream

A. Sollima<sup>1\*</sup>, E. Carretta<sup>1</sup>, V. D’Orazi<sup>2,3</sup>, R. G. Gratton<sup>4</sup>, A. Bragaglia<sup>1</sup>, S. Lucatello<sup>4</sup>

<sup>1</sup> *INAF Osservatorio Astronomico di Bologna, via Ranzani 1, Bologna, 40127, Italy*

<sup>2</sup> *Department of Physics and Astronomy, Macquarie University, Balaclava Road, North Ryde, NSW 2109, Australia*

<sup>3</sup> *Monash Centre for Astrophysics, School of Mathematical Sciences, Monash University, Building 28, Clayton, VIC 3800, Australia*

<sup>4</sup> *INAF Osservatorio Astronomico di Padova, vicolo dell’Osservatorio 5, Padova, 35122, Italy*

24 March 2022

## ABSTRACT

We present the results of a spectroscopic survey of Red Giants in the globular cluster Terzan 8 with the aim of studying its kinematics. We derived accurate radial velocities for 82 stars located in the innermost 7′ from the cluster center identifying 48 bona fide cluster members. The kinematics of the cluster have been compared with a set of dynamical models accounting for the effect of mass segregation and a variable fraction of binaries. The derived velocity dispersion appears to be larger than that predicted for mass-segregated stellar systems without binaries, indicating that either the cluster is dynamically young or it contains a large fraction of binaries (>30%). We detected 7 stars with a radial velocity compatible with the cluster systemic velocity but with chemical patterns which stray from those of both the cluster and the Galactic field. These stars are likely members of the Sagittarius stream surrounding this stellar system.

**Key words:** methods: data analysis – methods: statistical – techniques: spectroscopic – stars: kinematics and dynamics – stars: Population II – globular clusters: individual: Terzan 8

## 1 INTRODUCTION

The globular cluster (GC) Terzan 8 is one of the faintest GCs populating the outer halo. Discovered by Terzan (1968), it is located at a distance of 19.4 kpc from the Galactic center in the constellation of Sagittarius ( $RA = 19^h 41^m 44.41^s$ ,  $Dec = -33^\circ 59' 58.1''$ ; Harris 1996, 2010 edition). The photometric studies of this GC (Ortolani & Gratton 1990; Montegriffo et al. 1998) suggested that it is an old, metal-poor object with a blue Horizontal Branch (HB). The first spectroscopic study of this cluster analysed 3 Red Giant stars in the CaII triple region and derived a very low metallicity ( $[Fe/H]=-2.3$ ; Da Costa & Armandroff 1985). More recently, Mottini, Wallerstein & McWilliam (2008) used high-resolution spectroscopy to determine abundances of Fe, O, Na,  $\alpha$ -, Fe-peak, and neutron-capture elements for 3 Red Giants. The small number of targets of the above studies did not allow a relevant analysis of the cluster kinematics. Recently, we performed an high-resolution spectroscopic survey of this cluster (Carretta et al. 2014) providing accurate ra-

dial velocities for 82 stars in the central region of the cluster and abundances of 16 members.

From the dynamical point of view, Terzan 8 is the less concentrated GC of the Milky Way ( $c=0.41$ ) and it appears very extended (with an half-light radius of 15.3 pc; Salinas et al. 2011). Such a peculiar structure implies a half-mass relaxation time comparable with its age, suggesting that Terzan 8 could be dynamically young.

The interest for this cluster increased because of its probable association with the Sagittarius dwarf galaxy (Ibata, Gilmore & Irwin 1994). Indeed, the location in the sky, radial velocity and distance of Terzan 8 are consistent with that of this satellite galaxy (Da Costa & Armandroff 1995; Dinescu et al. 2001; Palma, Majewski & Johnston 2002; Bellazzini et al. 2003; Majewski et al. 2004; Carraro, Zinn & Moni Bidin 2007). In particular, N-body simulations indicate that Terzan 8 could be immersed in the trailing arm of the Sagittarius stream (Edelsohn & Elmegreen 1997; Law & Majewski 2010). Moreover, the presence of the Sagittarius stream has been detected as an overdensity of stars in a wide region surrounding this cluster (Giuffrida et al. 2010; Siegel et al. 2011).

In this paper we use the radial velocities obtained in the

\* E-mail: antonio.sollima@oabo.inaf.it

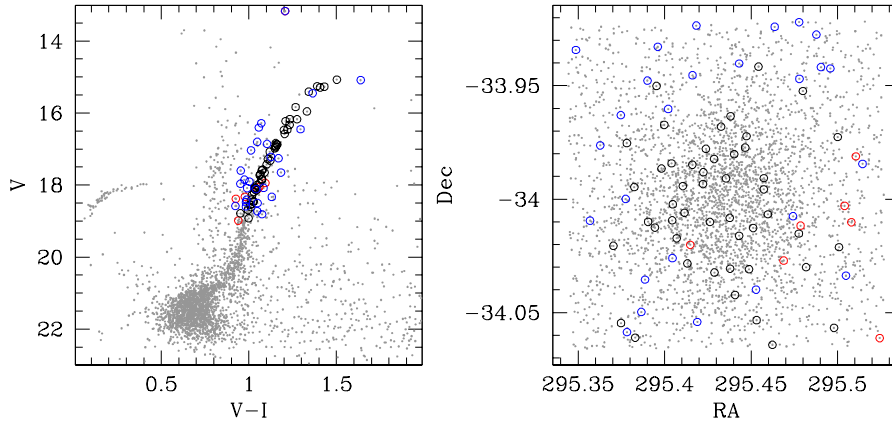


**Figure 1.** V,V-I color-magnitude diagram (left panel) and map (right panel) of Terzan 8 (grey points; from Montegriffo et al. 1998). In both panels black, blue and red dots (asterisks, open and filled dots in the printed version of the paper) represent the observed cluster members, field stars and Sagittarius stars, respectively.

survey by Carretta et al. (2014) to investigate the kinematics of Terzan 8. In Sect. 2 we describe the observational material and the data reduction procedure. Sect. 3 is devoted to the comparison of the derived velocity dispersion with a set of dynamical models. In Sect. 4 we discuss the spectroscopic signature of the surrounding Sagittarius stream. We summarize and discuss our results in Sect. 5.

## 2 OBSERVATIONS AND DATA REDUCTION

Spectra have been obtained using the multi-object spectrograph VLT/FLAMES (Pasquini et al. 2002). A more detailed description of the observations and analysis is presented in Carretta et al. (2014). We give here only a short description. We used the Ultraviolet and Visual Echelle Spectrograph (UVES) 580 nm setup (4800 – 6800Å; with a spectral resolution of  $R \sim 45000$ ) and the GIRAFFE high-resolution setups HR11 and HR13, providing a spectral resolution of  $R \sim 24200$  and 22500, respectively. The target stars have been selected from the photometric catalog by Montegriffo et al. (1998) covering a region of  $9.15' \times 8.6'$  centered on the cluster. We selected seven among the brightest Red Giant Branch (RGB) stars for the UVES fibres ( $R \sim 45000$ ) while the GIRAFFE fibres were allocated to objects on or near the RGB (84 stars) or the HB (17 stars; see Fig. 1). A set of  $6 \times 4720$  sec exposures have been obtained. Unfortunately, because of the instrumental setup, the low metallicity and S/N, we could not measure radial velocities for 2 RGB and all HB stars. The observations were obtained in service mode under seeing conditions of  $0.7'' < FWHM < 2.2''$ . The spectra were reduced (bias and flat-field corrected, 1D extracted, and wavelength calibrated) using the ESO pipeline. We applied sky subtraction and division by an observed early-type star (UVES), or a synthetic spectrum (GIRAFFE) to correct for telluric features near the [OI] line using the IRAF routine telluric. The latter correction was applied only to the UVES and bright GIRAFFE samples. We shifted all spectra according

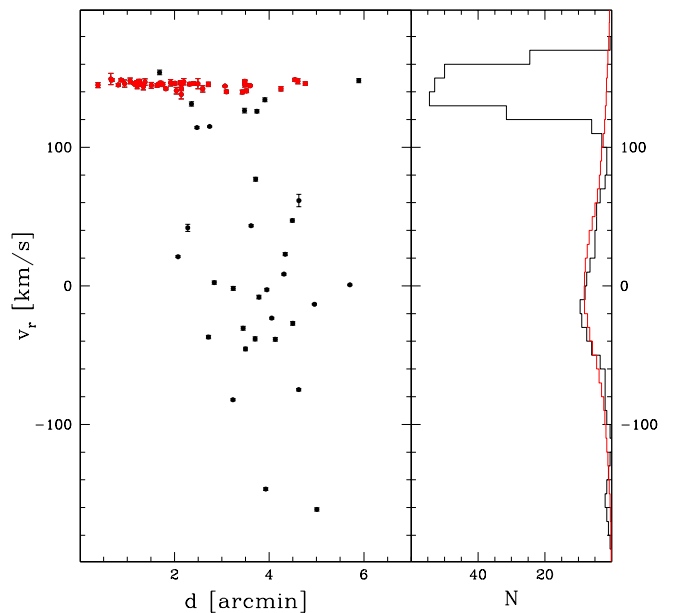


**Figure 2.** Radial velocities of the target stars as a function of the distance from the cluster center (left panel). Red points (filled dots in the printed version of the paper) mark the bona fide cluster members (see Sect. 3). In the right panel the distribution of radial velocities is shown. The prediction of the Galactic model of Robin et al. (2003) is shown with red histograms (grey in the printed version of the paper).

to their heliocentric velocity and combined the individual exposures. The UVES final spectra have S/N in the range 45-80 while the GIRAFFE spectra have S/N values ranging from 5 to 80. The heliocentric radial velocities and their uncertainties were then measured on the combined spectra of 82 stars using the IRAF task rvidlines. Uncertainties have been calculated from the r.m.s. of the velocities measured

using different lines. They are listed in Table 2 of Carretta et al. (2014).

In Fig. 2 the radial velocities of the observed stars are plotted as a function of the distance from the cluster center. The signal of Terzan 8 is clearly visible as a group of stars with velocity  $v_r \sim 142$  km/s and a small ( $< 2$  km/s) dispersion. The Galactic field population is also clearly identifiable at velocities  $v_r < 100$  km/s. We note that at  $v_r > 100$  km/s, besides the group of cluster members, other 8 stars have velocities similar to that of Terzan 8 but with a larger spread. Seven of them are located in the color-magnitude diagram (CMD) close to the cluster RGB, while one of them is clearly a bright field star at  $V < 14$  (see Fig. 1). Curiously, all these 7 stars are located in the same half of the observed field of view. All these stars were observed with GIRAFFE.

For 5 out of these 7 stars we derived the abundance of Fe (from both FeI and FeII lines), Mg, Si, Ca, Ti, Ba from their spectra. The other two stars have a faint magnitude ( $V > 18.5$ ) and the low S/N ( $\sim 20$ ) of their spectra do not allow a reliable estimation of their abundances. We performed the analysis as described in Carretta et al. (2014). Temperatures have been derived using the V-I color-temperature relation by Alonso, Arribas & Martínez-Roger (1999) and the reddening  $E(B-V)=0.12$  (Schlegel, Finkbeiner & Davis 1998; Harris catalog). Gravities have been derived using the universal gravitation law assuming a mass of  $0.85 M_\odot$  (suitable for a Red Giant) and a luminosity calculated converting the V band into bolometric magnitude using the corrections by Alonso et al. (1999), and assuming the apparent distance modulus of Terzan 8 ( $m - M)_V = 17.47$  (from the Harris catalog), the above mentioned reddening and a solar bolometric magnitude of  $M_{bol,\odot} = 4.75$ . Microturbulence velocities have been calculated as a function of gravities using the relation by Worley et al. (2013). We interpolated within the Kurucz (1993) grid of model atmospheres (with the option for overshooting turned on) and tuned the abundances of the various elements to match the equivalent widths of several lines.

### 3 KINEMATICS

#### 3.1 Overall velocity dispersion, density profile and mass function

To study the structure and kinematics of Terzan 8 we derived its overall velocity dispersion, its density profile and its luminosity function (MF). As a first step, we selected a sample of bona fide cluster members on the basis of their locations in the CMD and their radial velocities. In particular, we considered only those stars with

- a location in the CMD within  $\Delta(V - I) < 0.1$  around the cluster RGB mean ridge line and a magnitude within  $14 < V < 19$ ;
- a radial velocity within  $5\sigma$  from the mean systemic velocity.

According to the above criteria we defined a sample of 48 members. The average radial velocity turns out to be  $\langle v_r \rangle = 145.26 \pm 0.15$  km/s (where the reported uncertainty is the error on the mean, while r.m.s.=2.46 km/s). For comparison, Da Costa & Armandroff (1995) reported an average

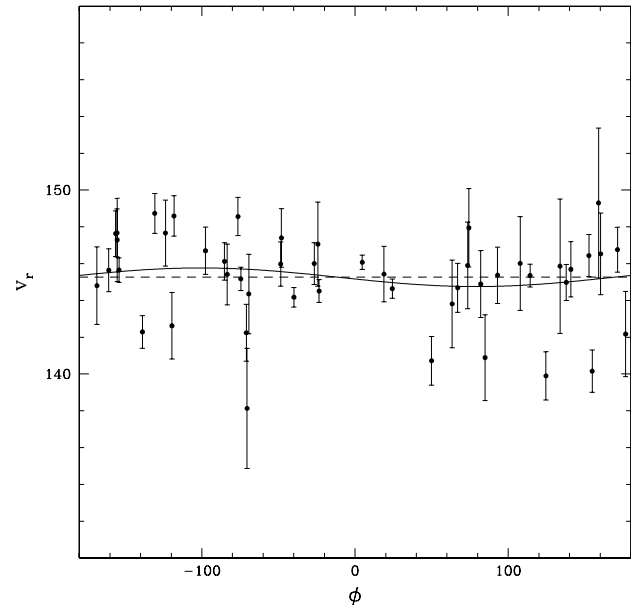


**Figure 3.** Radial velocity of the 48 member stars of Terzan 8 as a function of the position angle. The best-fit sinusoidal trend and the mean radial velocity are marked with solid and dashed lines, respectively.

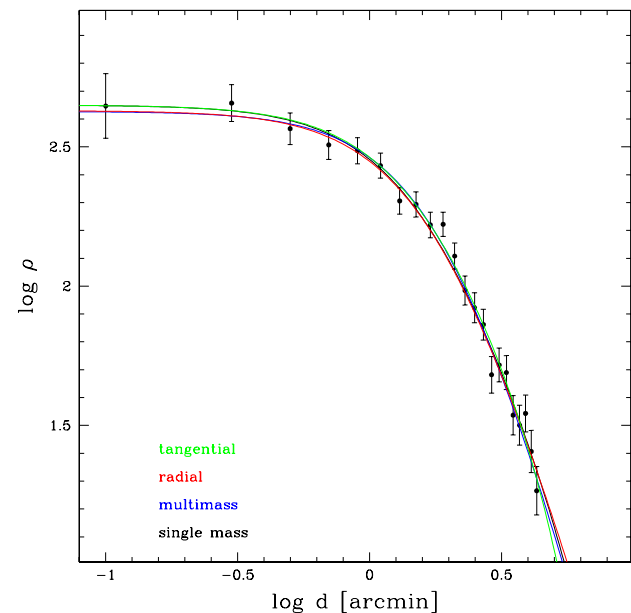


**Figure 4.** Density profile of Terzan 8. The prediction of the various models are overplotted.

radial velocity  $\langle v_r \rangle = 130 \pm 8$  from the analysis of three stars. The star-to-star comparison with our catalog gives a perfect agreement and the difference in the average velocity is probably due to their very small sample. We cannot compare our values with the study of Mottini et al. (2008) because they do not provide the radial velocities for their targets.

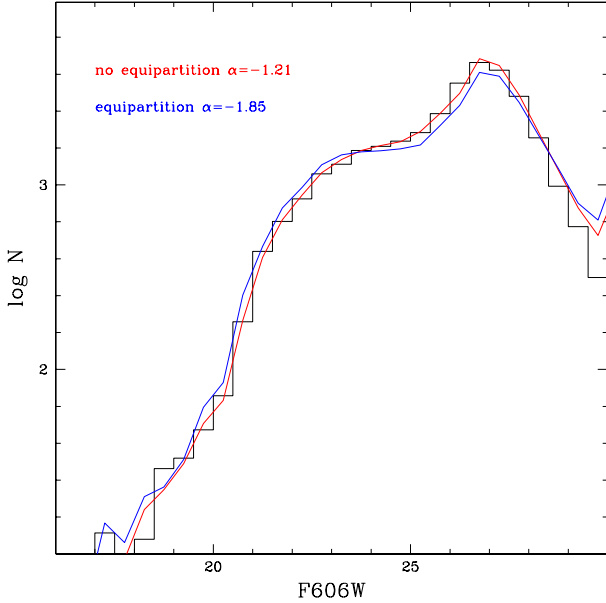


**Figure 5.** F606W luminosity function of Terzan 8 (black histograms). The prediction of models with and without kinetic energy equipartition are also marked with red and blue lines (black and grey in the printed version of the paper), respectively.

The overall velocity dispersion has been calculated using the algorithm proposed by Pryor & Meylan (1993), where the velocity dispersion is calculated as the quantity  $\sigma_v$  that maximizes the likelihood

$$\begin{aligned}
 l &= \sum_i \ln \int_{-\infty}^{+\infty} \frac{\exp \left[ -\frac{(v' - \bar{v})^2}{2\sigma_v^2} - \frac{(v_i - v')^2}{2\delta_i^2} \right]}{2\pi\sigma_v\delta_i^2} dv' \\
 &= -\frac{1}{2} \sum_i \left( \frac{(v_i - \bar{v})^2}{\sigma_v^2 + \delta_i^2} + \ln[2\pi(\sigma_v^2 + \delta_i^2)] \right) \quad (1)
 \end{aligned}$$

where  $v_i$  and  $\delta_i$  are the velocity of the  $i$ -th star and its associated uncertainty. The calculated velocity dispersion turns out to be  $\sigma_v = 1.72 \pm 0.14$  km/s. Unfortunately, because of the small number of target stars it is not possible to construct a reliable velocity dispersion profile. In Fig. 3 the radial velocities of the bona fide cluster members are plotted as a function of the position angle. The distribution appears homogeneous and no clear trend is apparent. A fit with a sinusoidal curve indicates a maximum rotation amplitude of  $v_{rot,max} \sin i = 0.50 \pm 0.21$  km/s consistent with no significant rotation along the line-of-sight within Terzan 8.

The density profile has been constructed from the photometric catalog by Montegriffo et al. (1998) by dividing the number of stars brighter than  $V < 21$  and contained in circular annuli by the annulus area. We adopted the above magnitude limit to ensure a significant number of stars with a completeness level  $>90\%$ , as estimated through artificial star experiments. The derived density profile is shown in Fig. 4.

The luminosity function of the cluster has been derived using the deep ACS@HST photometry provided by the ACS treasury project (Sarajedini et al. 2007). These data cover a region of  $202'' \times 202''$  around Terzan 8 and

provide a deep CMD in the F606W and F814W filters down to  $F666W \sim 28$ . A detailed description of the photometric reduction, astrometry, and artificial star experiments for this database can be found in Anderson et al. (2008). We selected Main Sequence stars by selecting stars within 3 times the standard deviation of the median F666W-F814W color at a given F606W magnitude. The F606W luminosity function has been then calculated by counting stars in bins of magnitudes of 0.5 mag width and it is shown in Fig. 5.

### 3.2 Models

We compared the overall velocity dispersion of Terzan 8 as measured in our sample with the prediction of a set of dynamical models taking into account the location of targets across the field of view.

In principle, in relaxed stellar systems the most massive RGB stars are kinematically colder than low-mass stars. Therefore, since our velocity dispersion is calculated only for RGB stars, we should take into account this effect. However, given the long relaxation time of Terzan 8 it is possible that the cluster has still not reached a significant degree of kinetic energy equipartition. In this case, stars with different masses would follow the same velocity dispersion profile.

Therefore, we considered a set of single-mass King (1966) and multi-mass King-Michie models (Gunn & Griffin 1979). For single-mass models we also considered two extreme degrees of radial and tangential anisotropy using the formalism by Gunn & Griffin (1979; we assumed the criterion for stability by Nipoti, Londrillo & Ciotti 2002). For multi-mass models we considered 8 mass bins between 0.1 and  $0.9 M_\odot$  having a width of  $0.1 M_\odot$  each.

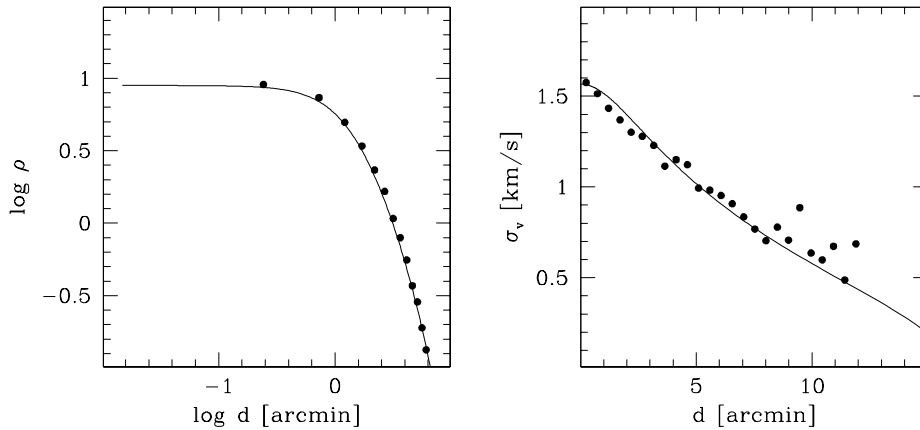
Dark remnants have been added using the initial-final mass relation and the retention fractions by Kruijssen (2009). We adopted for the dark remnants the same MF of the other stars.

A population of binaries has been also added by calculating the projected velocity component of a  $0.85 M_\odot$  primary star in a binary systems with a given period, eccentricity and inclination angles (McConnachie & Côté 2010). For this purpose, the secondary masses have been randomly extracted from a uniform distribution between  $0.1 < M/M_\odot < 0.85$ . A period has been then extracted from the log-normal distribution of Duquennoy & Mayor (1991) truncated at the periods corresponding to the limiting semi-major axes  $a_{min}$  and  $a_{max}$ . The value of  $a_{min}$  has been chosen as the minimum distance at which mass-transfer between the components would occur (Lee & Nelson 1988) while for  $a_{max}$  has been chosen the value for which the binding energy of the binary equates the mean kinetic energy of clusters stars ( $\langle m\sigma_v^2 \rangle$ ). The eccentricity has been chosen following the prescription of Duquennoy & Mayor (1991). We adopted a random distribution of orbital phases, inclination angles and longitudes of the periastron.

For each model, we searched for the parameters (central adimensional potential  $W_0$ , MF slope  $\alpha$ , and core radius  $r_c$ ) which bestfit the observed density profile shown in Fig. 4. A synthetic CMD has been constructed by interpolating across the set of tracks by Dotter et al. (2007) with appropriate metallicity and age and adopting the distance modulus and reddening described in Sect. 2. Stars have been distributed across the cluster according to the density pro-

**Table 1.** Properties of the adopted dynamical models.

model	equipartition	$r_a$ pc	$W_0$	$r_h$ pc	$\alpha$	$\xi$ %	$\log M/M_\odot$	$\langle\sigma_v\rangle$ km/s	$t_{rh}$ Gyr	$(M/L_V)_{dyn}$ $M_\odot/L_\odot$
s_iso_fb0	no	$\infty$	5.0	24.36	-1.21	0	4.95	1.49	1.99	1.2
s_iso_fb20	no	$\infty$	5.0	24.36	-1.21	20	4.95	1.61	1.99	1.1
s_iso_fb40	no	$\infty$	5.0	24.36	-1.21	40	4.95	1.75	1.99	0.9
s_rad_fb0	no	23.36	4.0	26.72	-1.21	0	5.00	1.52	2.38	1.2
s_tan_fb0	no	36.00	5.0	22.68	-1.21	0	4.93	1.48	1.75	1.3
m_iso_fb0	yes	$\infty$	9.0	43.44	-1.85	0	4.97	1.06	7.47	7.4
m_iso_fb20	yes	$\infty$	9.0	43.44	-1.85	20	4.97	1.24	7.47	5.4
m_iso_fb40	yes	$\infty$	9.0	43.44	-1.85	40	4.97	1.43	7.47	4.1

**Figure 6.** Projected density (left panel) and velocity dispersion (right panel) profiles calculated from the last snapshot of the N-body simulation. The quantities at the end of the simulation are marked by filled dots. The best-fit static King (1966) model is overplotted in both panels with solid lines.

file of their mass bin. The F606W luminosity function of the synthetic CMD has been then estimated using the same technique described in Sect. 3.1 after correcting for the completeness estimated through the large set of artificial stars experiments described in Anderson et al. (2008). We considered only those stars within a distance of  $200''$  from the cluster center. The slope of the MF has been then chosen to reproduce the observed F606W luminosity function. We adopted the algorithm described in Sollima, Bellazzini & Lee (2012) to derive the bestfit parameters through an iterative procedure.

The cluster mass has been then calculated by matching the number of stars brighter than  $V < 20.5$  in the innermost  $5'$  of the photometric catalog by Montegriffo et al. (1998).

It is known that the interaction with the Milky Way tidal field can alter the velocity dispersion of the system by heating stars at large distances from the center (Küpper et al. 2010). To estimate the effect of tides we performed an N-body simulation to follow the structural and kinematical evolution of a cluster with the orbital and structural characteristics of Terzan 8. We used the last version of the collisionless N-body code *gyrfalcON* (Dehnen 2000). The cluster has been represented by 10,000 particles distributed according to the best-fit King (1966) model. The mean masses of the particles have been scaled to match the cluster mass pre-

dicted by this model. We adopted a leapfrog scheme with a time step of  $\Delta t = 5.82 \times 10^4$  yr and a softening length of 0.12 pc (following the prescription of Dehnen & Read 2011). Such a relatively large time step and softening length do not affect the accuracy of the simulation because we are interested in the tidal effects that occur on a timescale significantly shorter than the relaxation time (the timescale at which collisions become important). The cluster was launched within the three-component (bulge + disk + halo) static Galactic potential of Johnston, Spergel & Hernquist (1995) on a quasi-circular orbit starting from its present-day location and its evolution has been followed for 1.2 Gyr (corresponding to two orbital periods). The projected density and velocity dispersion profiles at the end of the simulation are shown in Fig. 6. It is apparent that both the density and the velocity dispersion profile of the cluster are almost unaffected by the presence of the tidal field with only a hint of deviation from the prediction of the static model at distances  $d > 8'$ . It is also interesting to note that in spite of the extended structure of the cluster, the tidal field does not produce a significant distortion of the cluster structure within the field of view covered by our photometric observations (with an ellipticity  $\epsilon < 0.002$  within  $4.5'$  from the cluster center).

To calculate the overall velocity dispersion predicted by the various models we adopted the Monte Carlo approach

already applied in Sollima et al. (2012). In particular, for each model the following steps have been performed:

- We compute the distance of the star from the cluster center and extract a velocity from a Gaussian function with a standard deviation corresponding to the local line-of-sight (LOS) velocity dispersion in the model. When the N-body simulation has been considered, the projected velocity of the closest particle has been adopted;
- We extract a random velocity from a Gaussian distribution with dispersion  $\delta_i$  and sum it to the previous one to compute a simulated observational velocity;
- A random number between 0 and 1 is extracted from a uniform distribution. If this number is smaller than the adopted binary fraction ( $\xi$ ) a binary is randomly extracted from the library (see above) and its apparent velocity is added to the simulated velocity.

In this way, every realization contains the same number of objects at the same location as the observed sample. Finally, the velocity dispersion of the simulated sample is calculated using Eq. 1. The above procedure is repeated 1000 times to compute the distribution of predicted velocity dispersions. The outcome of all the simulations performed is summarized in Table 1.

### 3.3 Results

The distribution of predicted LOS velocity dispersions for the considered models are compared with the observed measure in Fig. 7 (bottom panels). It is apparent that the model without binaries and accounting for the effect of mass segregation predicts a velocity dispersions which is significantly smaller than the observed value of Terzan 8. The observed discrepancy can be overcome assuming a large fraction of binaries ( $\xi > 30\%$ ). It is also interesting to note that a very steep MF has been derived in this case ( $\alpha = -1.85 \pm 0.15$ ; for reference a Salpeter 1955 MF has slope  $\alpha = -2.35$  and the slopes derived for 17 GCs by the comprehensive study by Paust et al. 2010 range between -0.32 and -1.69).

A different situation is apparent when models without equipartition are considered: in this case models with a moderate fraction of binaries predict velocity dispersion compatible within the errors with the observed value. In this case, the derived MF slope turns out to be  $\alpha = -1.21 \pm 0.09$ .

There is no appreciable difference between the best-fit single-mass King (1966) model in isolation and the Nbody simulation within the Milky Way tidal field (see the top-left panel of Fig. 7). This is expected since the small deviations from the prediction of the isolated models occurs only at distance larger than the radial coverage of the target stars.

In the same way, models with different degrees of anisotropy predict similar velocity dispersions (see the top-right panel of Fig. 7). This is due to the distribution of the target stars within the field of view: in the region where most of the observed stars reside, models with different anisotropies predict very similar velocity dispersion profiles.

## 4 THE SAGITTARIUS STREAM AROUND TERZAN 8

As already reported in Sect. 2, a group of 7 stars located close to the RGB of Terzan 8 with a similar systemic velocity but a larger spread are present. These stars could be either *i*) binary stars of Terzan 8, *ii*) Galactic field interlopers, or *iii*) stars belonging to the Sagittarius stream surrounding Terzan 8.

We compared the observed distribution of velocities with the Galactic model of Robin et al. (2003). For this purpose, a synthetic catalog covering 1 sq.deg. centered at the cluster location has been retrieved. We selected only stars which lie in the CMD brighter than  $V < 19$  and within  $\Delta(V - I) < 0.1$  about the RGB mean ridge line and normalized the sample to reproduce the observed number of stars at  $v_r < 100$  km/s (where only the Galactic field population is expected to be present). The model predicts a contamination of 3.7 stars at  $v_r > 100$  km/s. Note that all the synthetic field stars in this velocity range are Main Sequence stars in the foreground of the cluster. Unfortunately, the time coverage of our spectra does not allow to identify binaries from their velocity variation, so the only chance to distinguish them from cluster members and the field population is to use their chemistry.

The derived abundances of Fe,  $\alpha$ -elements and Ba for the 5 stars of this sample with sufficient S/N are listed in Table 2. In Fig. 8 they are compared with the sample of field giants analysed by Gratton et al. (2003) and Venn et al. (2004), Terzan 8 stars by Carretta et al. (2014) and Sagittarius stars by Carretta et al. (2010) and Sbordone et al. (2007). In spite of the large uncertainties on the derived abundances it is clear that the 5 stars have a metallicity which is not consistent with that of Terzan 8: they span a wide range  $-1.44 < [Fe/H] < -0.83$  being significantly more metal-rich than the cluster members (at  $[Fe/H] \sim -2.3$ ). The comparison with the field Milky Way and Sagittarius stars is less clear and is hampered by the large uncertainties in the derived abundances. However, we note that while the abundances of Si and Ca are consistent with those of both groups, the mean Ti I and Mg abundance are significantly lower than those of the Galactic giants while still compatible with those of Sagittarius<sup>1</sup>. Moreover, Ba appears to be enhanced by  $\sim 0.3$  dex in 4 of them, in agreement with what observed in Sgr stars (Sbordone et al. 2007). Even more important is the excellent agreement between the abundance of Fe measured from the neutral and ionized lines in all the analysed stars. As stated in Sect. 2 we adopted a gravity derived assuming these objects as RGB stars at the same distance of Terzan 8. Were these stars foreground Milky Way dwarfs their gravity would be larger by  $\Delta \log g > 1$ . According to the sensibility reported in Carretta et al. (2014) this would produce a striking mismatch between the abundances of Fe I and Fe II as a consequence of the wrong adopted ionization equilibrium. On the basis of the above considerations we conclude that at least 4 out these 7 stars are likely member of the Sagittarius stream.

<sup>1</sup> The Mg abundances of three stars (#47, #57, #65) lie  $\sim 0.4 - 0.6$  dex ( $\sim 2 \sigma$ ) below the mean locus of Sgr stars. Given the large involved uncertainties it is not clear whether this difference is real or due to measurement errors.

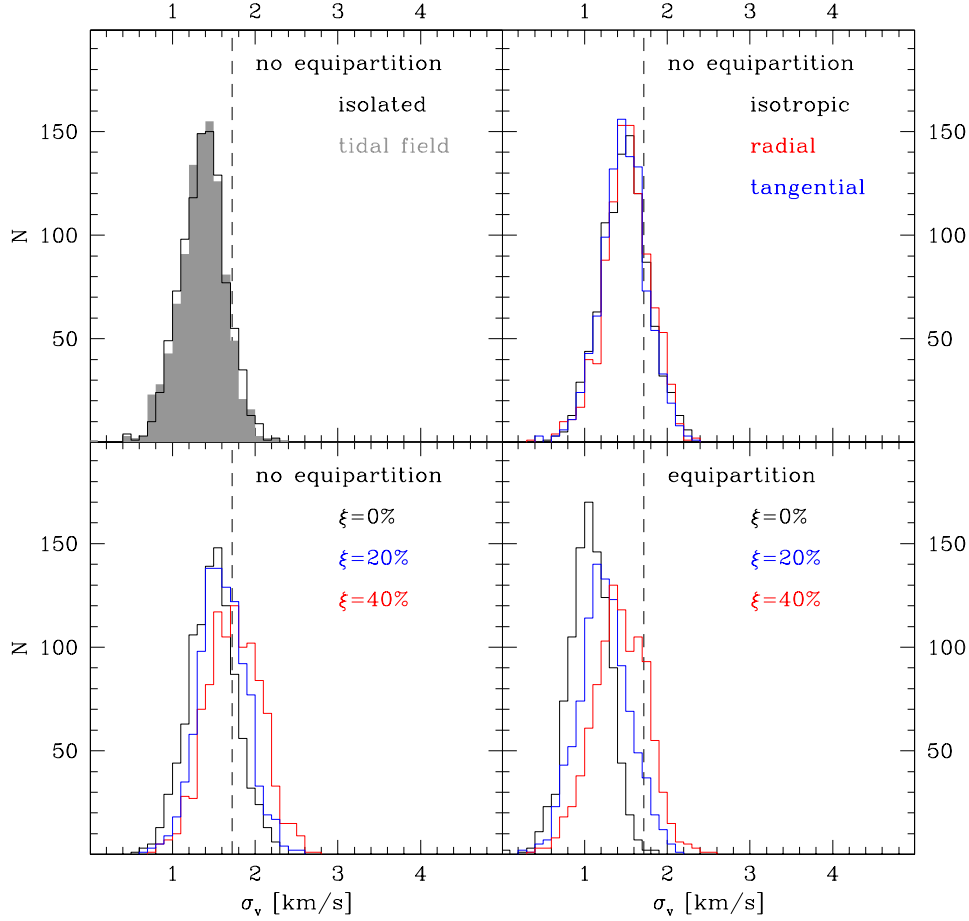


**Figure 7.** Predicted velocity dispersion of the considered dynamical models. In the bottom panels models without (bottom-right panel) and with (bottom-left panel) kinetic energy equipartition and different fraction of binaries are compared. In the top-left panel the distributions of the isolated model and the N-body simulation within the tidal field are compared. In the top-right panel two models with different degrees of anisotropy are compared. The observed velocity dispersion is marked with a dashed line in all panels.

**Table 2.** Abundances of the Sgr stars.

ID	[Fe I/H]	[Fe II/H]	[Mg/Fe]	[Si/Fe]	[Ca/Fe]	[Ti I/Fe]	[ $\alpha$ /Fe]	[Ba/Fe]
41	-1.44 ( $\pm 0.26$ )	-1.43 ( $\pm 0.36$ )	0.27 ( $\pm 0.30$ )	0.40 ( $\pm 0.20$ )	0.29 ( $\pm 0.17$ )	-0.05 ( $\pm 0.10$ )	0.23 ( $\pm 0.19$ )	-0.18 ( $\pm 0.30$ )
47	-0.83 ( $\pm 0.34$ )	-0.86 ( $\pm 0.38$ )	-0.17 ( $\pm 0.10$ )	0.17 ( $\pm 0.32$ )	0.33 ( $\pm 0.28$ )	-0.02 ( $\pm 0.10$ )	0.08 ( $\pm 0.22$ )	0.43 ( $\pm 0.30$ )
57	-0.84 ( $\pm 0.35$ )	-0.85 ( $\pm 0.10$ )	-0.08 ( $\pm 0.30$ )	0.29 ( $\pm 0.13$ )	0.30 ( $\pm 0.16$ )	-0.08 ( $\pm 0.28$ )	0.11 ( $\pm 0.22$ )	0.36 ( $\pm 0.30$ )
65	-1.08 ( $\pm 0.35$ )	-1.16 ( $\pm 0.30$ )	-0.36 ( $\pm 0.30$ )	0.29 ( $\pm 0.16$ )	0.11 ( $\pm 0.29$ )	0.04 ( $\pm 0.10$ )	0.02 ( $\pm 0.28$ )	0.27 ( $\pm 0.30$ )
70	-1.14 ( $\pm 0.39$ )	-1.11 ( $\pm 0.31$ )	0.16 ( $\pm 0.30$ )	0.39 ( $\pm 0.43$ )	0.24 ( $\pm 0.24$ )	0.67 ( $\pm 0.18$ )	0.37 ( $\pm 0.22$ )	0.26 ( $\pm 0.30$ )

## 5 CONCLUSIONS

We performed a detailed study of the structure and kinematics of the GC Terzan 8 by means of a set of accurate radial velocities obtained through high-resolution spectroscopy in the inner part of the cluster.

The cluster density profile is well fitted by very extended models with the largest half-mass radius among Galactic

GCs ( $22 < r_h/pc < 44$ ). By considering the estimated mass and the Galactocentric distance of this GC we estimate an half mass-to-Jacobi radii ratio of  $r_h/r_J \sim 0.16$ . In comparison with the other Galactic GCs it situates in the upper branch of the  $r_h/r_J$  vs.  $R_{GC}$  diagram constituted by extended low-mass GCs (Baumgardt et al. 2010). The position of these clusters has been interpreted as a consequence

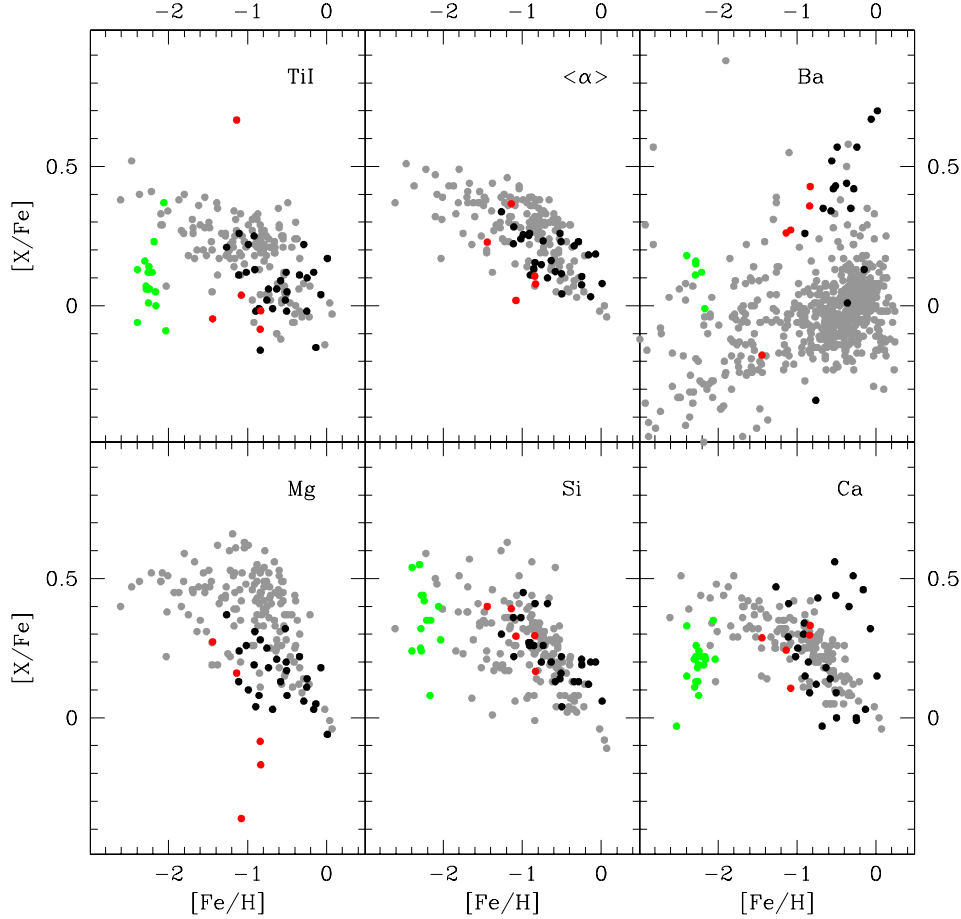


**Figure 8.** Abundance patterns of the  $\alpha$ -elements and Ba in the 5 stars suspected to belong to the Sagittarius stream (red dots; open stars in the printed version of the paper). The abundances of the field giants (grey dots; from Gratton et al. 2003 and Venn et al. 2004), Sagittarius stars (black dots; from Carretta et al. 2010 and Sbordone et al. 2007) and Terzan 8 stars (green dots, open dots in the printed version of the paper; from Carretta et al. 2014) are also plotted.

of different cloud pressure and background tidal force at their formation (Elmegreen 2008). It is interesting to note that many of these clusters have been associated to merging dwarf galaxies. It is not clear if Terzan 8 was born with such an extended structure or this is due to its dynamical evolution, although its long relaxation time suggests the former hypothesis. In this context, if Terzan 8 spent most of its evolution within a dwarf galaxy (like the Sagittarius dSph) it experienced a mild tidal field and could therefore form and evolve with a more extended structure with respect to other GCs formed within the Milky Way halo. This could explain also the small fraction of Na-enhanced stars found in this cluster (see Carretta et al. 2014). These stars are indeed expected to form in the central part of the cluster after some  $10^{6-7}$  yrs after the cluster formation being more resistant than the first stellar generation to the tidal stripping process (D’Ercole et al. 2008; Decressin et al. 2007). For this reason, while in GCs the first stellar generation generally constitute only a small fraction of the cluster content, in Terzan 8 it is almost entirely retained in Terzan 8 because of the mild tidal stress experienced by this cluster.

We found no significant radial component of rota-

tion within the cluster, although slow rotations (with  $v_{rot} \sin i / \sigma_v < 0.4$ ) would not be detected by our study and cannot therefore be excluded.

The derived overall velocity dispersion appears to be larger than what predicted by dynamical models assuming kinetic energy equipartition and a moderate amount of binaries. On the other hand, models without equipartition can reproduce the observed velocity dispersion regardless of the adopted fraction of binaries. The half-mass relaxation times of the considered models are  $1.7 < t_{rh} / \text{Gyr} < 7.5$ , shorter than the estimated cluster age ( $t_9 = 12.2$  Gyr; Marín-Franch et al. 2009). It is therefore unlikely that collisional effects have not altered the kinematics of this GC. By means of Nbody simulations we estimated only a negligible contribution of tidal effects to the cluster velocity dispersion, at least when quasi-circular orbits are considered. In principle, highly eccentric orbits could produce a more significant inflation of the velocity dispersion even in the innermost regions of the clusters. Such a hypothesis requires a specific study with extensive Nbody simulations. The observed discrepancy could be eliminated if a large fraction ( $\xi > 30\%$ ) of binaries is present within Terzan 8. Unfortunately, the



time coverage of our spectra does not allow to identify binaries from their velocity variation. An estimate of the binary fraction in this cluster has been provided by Milone et al. (2012) who found  $\xi = 13.4\%$  within the ACS field of view. It is worth noting that the uncertainties in the adopted distribution of periods, eccentricity and mass-ratios of binaries affect the determination of the binary fraction through photometric and spectroscopic studies in different ways and can produce a mismatch between these two estimates. It is also interesting to note that the masses of the models have been calculated from the number counts on the CMD and can be therefore considered as an estimate of the luminous mass of this cluster. The large observed velocity dispersion could be viewed as an excess of dynamical mass within Terzan 8, as indicated by the large dynamical mass-to-light ratios  $(M/L_V)_{dyn} > 4$ . A systematic difference between the luminous and dynamical masses of many GCs have been already noticed by Sollima et al. (2012) who addressed the observed difference to the large uncertainties on the MF and the retention fraction of dark remnants. Also in this case, different assumptions on the dark remnants could alleviate or even eliminate the difference between the observed and predicted velocity dispersion of this GC.

We detected a sample of 7 stars with radial velocities in the range  $100 < v_r < 200$  km/s apparently clustered around the systemic velocity of Terzan 8 but with a spread significantly larger than the cluster velocity dispersion. These stars are spatially segregated with respect to the other field and cluster stars occupying the same half of the observed field of view. The probability that this occurs by chance is  $\sim 0.8\%$ . The abundance analysis performed on these stars indicates that they have a metallicity which is inconsistent with that of the cluster. The abundance patterns of the  $\alpha$ -elements and Ba indicate a deficiency of Mg and Ti I and an overabundance of Ba in these stars with respect to Galactic field stars and more similar to those measured in Sagittarius stars. Moreover, the gravities estimated for these stars are consistent with a distance similar to that of Terzan 8. The comparison with the Galactic model of Robin et al. (2003) indicates that it is unlikely that a significant number of Galactic field stars could be present at such a large Galactocentric distance. We therefore conclude that they are likely member of the Sagittarius stream surrounding Terzan 8. The presence of the Sagittarius stream has been already detected in some previous studies based on wide field photometric surveys (Giuffrida et al. 2010; Siegel et al. 2011; Salinas et al. 2012). This however represents the first spectroscopic detection of Sagittarius stars around this GC, confirming its belonging to the stream of this satellite galaxy.

## ACKNOWLEDGMENTS

This research has been funded by PRIN INAF 2011 "Multiple populations in globular clusters: their role in the Galaxy assembly" (PI E. Carretta) and PRIN MIUR 2010-2011 "The Chemical and Dynamical Evolution of the Milky Way and Local Group Galaxies" (PI F. Matteucci). VD is an ARC Super Science Fellow. We thank the anonymous referee for his/her helpful comments and suggestions.

## REFERENCES

- Alonso A., Arribas S., Martínez-Roger C., 1999, *A&AS*, 140, 261
- Anderson J., et al., 2008, *AJ*, 135, 2055
- Baumgardt H., Parmentier G., Gieles M., Vesperini E., 2010, *MNRAS*, 401, 1832
- Bellazzini M., Ibata R., Ferraro F. R., Testa V., 2003, *A&A*, 405, 577
- Carraro G., Zinn R., Moni Bidin C., 2007, *A&A*, 466, 181
- Carretta E., Bragaglia A., Gratton R. G., D'Orazi V., Lucatello S., Sollima A., 2014, *A&A*, 561, A87
- Carretta E., et al., 2010, *A&A*, 520, A95
- Da Costa G. S., Armandroff T. E., 1995, *AJ*, 109, 2533
- D'Ercole A., Vesperini E., D'Antona F., McMillan S. L. W., Recchi S., 2008, *MNRAS*, 391, 825
- Decressin T., Meynet G., Charbonnel C., Prantzos N., Ekström S., 2007, *A&A*, 464, 1029
- Elmegreen B. G., 2008, *ApJ*, 672, 1006
- Dehnen W., 2000, *ApJ*, 536, L39
- Dehnen W., Read J. I., 2011, *EPJP*, 126, 55
- Dinescu D. I., Majewski S. R., Girard T. M., Cudworth K. M., 2001, *AJ*, 122, 1916
- Dotter A., Chaboyer B., Jevremović D., Baron E., Ferguson J. W., Sarajedini A., Anderson J., 2007, *AJ*, 134, 376
- Duquenois A., Mayor M., 1991, *A&A*, 248, 485
- Edelsohn D. J., Elmegreen B. G., 1997, *MNRAS*, 290, 7
- Giuffrida G., Sbordone L., Zaggia S., Marconi G., Bonifacio P., Izzo C., Szeifert T., Buonanno R., 2010, *A&A*, 513, A62
- Gratton R. G., Carretta E., Claudi R., Lucatello S., Barbieri M., 2003, *A&A*, 404, 187
- Gunn J. E., Griffin R. F., 1979, *AJ*, 84, 752
- Harris W. E., 1996, *AJ*, 112, 1487
- Ibata R. A., Gilmore G., Irwin M. J., 1994, *Natur*, 370, 194
- Johnston K. V., Spergel D. N., Hernquist L., 1995, *ApJ*, 451, 598
- King I. R., 1966, *AJ*, 71, 64
- Kruijssen J. M. D., 2009, *A&A*, 507, 1409
- Küpper A. H. W., Kroupa P., Baumgardt H., Heggie D. C., 2010, *MNRAS*, 407, 2241
- Kurucz R. L., 1993, *PhST*, 47, 110
- Law D. R., Majewski S. R., 2010, *ApJ*, 718, 1128
- Lee H. M., Nelson L. A., 1988, *ApJ*, 334, 688
- Majewski S. R., et al., 2004, *AJ*, 128, 245
- Marín-Franch A., et al., 2009, *ApJ*, 694, 1498
- McConnachie A. W., Côté P., 2010, *ApJ*, 722, L209
- Milone A. P., et al., 2012, *A&A*, 540, A16
- Montegriffo P., Bellazzini M., Ferraro F. R., Martins D., Sarajedini A., Fusi Pecci F., 1998, *MNRAS*, 294, 315
- Mottini M., Wallerstein G., McWilliam A., 2008, *AJ*, 136, 614
- Nipoti C., Londrillo P., Ciotti L., 2002, *MNRAS*, 332, 901
- Ortolani S., Gratton R., 1990, *A&AS*, 82, 71
- Palma C., Majewski S. R., Johnston K. V., 2002, *ApJ*, 564, 736
- Pasquini L., et al., 2002, *Msngr*, 110, 1
- Paust N. E. Q., et al., 2010, *AJ*, 139, 476
- Pryor C., Meylan G., 1993, *ASPC*, 50, 357
- Robin A. C., Reylé C., Derrière S., Picaud S., 2003, *A&A*, 409, 523
- Salinas R., Jílková L., Carraro G., Catelan M., Amigo P.,

- 2012, MNRAS, 421, 960  
Salpeter E. E., 1955, ApJ, 121, 161  
Sarajedini A., et al., 2007, AJ, 133, 1658  
Sbordone L., Bonifacio P., Buonanno R., Marconi G.,  
Monaco L., Zaggia S., 2007, A&A, 465, 815  
Schlegel D. J., Finkbeiner D. P., Davis M., 1998, ApJ, 500,  
525  
Siegel M. H., et al., 2011, ApJ, 743, 20  
Sollima A., Bellazzini M., Lee J.-W., 2012, ApJ, 755, 156  
Terzan A., 1968, CRASB, 267, 1245  
Venn K. A., Irwin M., Shetrone M. D., Tout C. A., Hill V.,  
Tolstoy E., 2004, AJ, 128, 1177  
Worley C. C., Hill V., Sobeck J., Carretta E., 2013, A&A,  
553, A47